

Uniformly rotating neutron stars in the global and local charge neutrality cases

Riccardo Belvedere^{a,b}, Kuantay Boshkayev^d, Jorge A. Rueda^{a,b}, Remo Ruffini^{a,b,c}

^a*Dipartimento di Fisica and ICRA, Sapienza Universita' di Roma
P.le Aldo Moro 5, I-00185 Rome, Italy*

^b*ICRANet, P.zza della Repubblica 10, I-65122 Pescara, Italy*

^c*ICRANet, University of Nice-Sophia Antipolis, 28 Av. de Valrose, 06103 Nice Cedex 2, France*

^d*Physical-Technical Faculty, Al-Farabi Kazakh National University
Al-Farabi ave. 71, 050040 Almaty, Kazakhstan*

arXiv:1307.2836v2 [astro-ph.SR] 22 Nov 2013

Abstract

In our previous treatment of neutron stars, we have developed the model fulfilling global and not local charge neutrality. In order to implement such a model, we have shown the essential role by the Thomas-Fermi equations, duly generalized to the case of electromagnetic field equations in a general relativistic framework, forming a coupled system of equations that we have denominated Einstein-Maxwell-Thomas-Fermi (EMTF) equations. From the microphysical point of view, the weak interactions are accounted for by requesting the β stability of the system, and the strong interactions by using the σ - ω - ρ nuclear model, where σ , ω and ρ are the mediator massive vector mesons. Here we examine the equilibrium configurations of slowly rotating neutron stars by using the Hartle formalism in the case of the EMTF equations indicated above. We integrate these equations of equilibrium for different central densities ρ_c and circular angular velocities Ω and compute the mass M , polar R_p and equatorial R_{eq} radii, angular momentum J , eccentricity ϵ , moment of inertia I , as well as quadrupole moment Q of the configurations. Both the Keplerian mass-shedding limit and the axisymmetric secular instability are used to construct the new mass-radius relation. We compute the maximum and minimum masses and rotation frequencies of neutron stars. We compare and contrast all the results for the global and local charge neutrality cases.

1. Introduction

We have recently shown (Rotondo et al., 2011; Rueda et al., 2011; Belvedere et al., 2012) that the equations of Tolman-Oppenheimer-Volkoff (TOV) (Tolman, 1939; Oppenheimer and Volkoff, 1939), traditionally used to describe the neutron star equilibrium configurations, are superseded once the strong, weak, electromagnetic and gravitational interactions are taken into account. Instead, the Einstein-Maxwell system of equations coupled with the general relativistic Thomas-Fermi equations of equilibrium have to be used; what we called the Einstein-Maxwell-Thomas-Fermi (EMTF) system of equations. While in the TOV approach the condition of local charge neutrality, $n_e(r) = n_p(r)$ is imposed (see e.g. Haensel et al., 2007, and references therein), the EMTF approach requests the less stringent condition of global charge neutrality, namely

$$\int \rho_{ch} d^3r = \int e[n_p(r) - n_e(r)] d^3r = 0, \quad (1)$$

where ρ_{ch} is the charge density, e is the fundamental electric charge, and the integral is carried out on the entire volume of the system.

The Lagrangian density taking into account all the interactions include the free-fields terms \mathcal{L}_g , \mathcal{L}_γ , \mathcal{L}_σ , \mathcal{L}_ω , \mathcal{L}_ρ (respectively for the gravitational, the electromagnetic, and the three mesonic fields), the three fermion species (electrons, protons and neutrons) term \mathcal{L}_f and the interacting part in the minimal coupling assumption, \mathcal{L}_{int} (Rueda et al., 2011; Belvedere et al., 2012):

$$\mathcal{L} = \mathcal{L}_g + \mathcal{L}_f + \mathcal{L}_\sigma + \mathcal{L}_\omega + \mathcal{L}_\rho + \mathcal{L}_\gamma + \mathcal{L}_{int}, \quad (2)$$

where¹

$$\begin{aligned} \mathcal{L}_g &= -\frac{R}{16\pi}, \quad \mathcal{L}_f = \sum_{i=e,N} \bar{\psi}_i (i\gamma^\mu D_\mu - m_i) \psi_i, \\ \mathcal{L}_\sigma &= \frac{\nabla_\mu \sigma \nabla^\mu \sigma}{2} - U(\sigma), \quad \mathcal{L}_\omega = -\frac{\Omega_{\mu\nu} \Omega^{\mu\nu}}{4} + \frac{m_\omega^2 \omega_\mu \omega^\mu}{2}, \\ \mathcal{L}_\rho &= -\frac{\mathcal{R}_{\mu\nu} \mathcal{R}^{\mu\nu}}{4} + \frac{m_\rho^2 \rho_\mu \rho^\mu}{2}, \quad \mathcal{L}_\gamma = -\frac{F_{\mu\nu} F^{\mu\nu}}{16\pi}, \\ \mathcal{L}_{int} &= -g_\sigma \sigma \bar{\psi}_N \psi_N - g_\omega \omega_\mu J_\omega^\mu - g_\rho \rho_\mu J_\rho^\mu + e A_\mu J_{\gamma,e}^\mu \\ &\quad - e A_\mu J_{\gamma,N}^\mu, \end{aligned}$$

where the description of the strong interactions between the nucleons is made through the σ - ω - ρ nuclear model in

Email addresses: riccardo.belvedere@icra.it (Riccardo Belvedere), kuantay@icra.it (Kuantay Boshkayev), jorge.rueda@icra.it (Jorge A. Rueda), ruffini@icra.it (Remo Ruffini)

¹We use spacetime metric signature (+,-,-,-) and geometric units $G = c = 1$ unless otherwise specified.

the version of Boguta and Bodmer (1977). Thus $\Omega_{\mu\nu} \equiv \partial_\mu\omega_\nu - \partial_\nu\omega_\mu$, $\mathcal{R}_{\mu\nu} \equiv \partial_\mu\rho_\nu - \partial_\nu\rho_\mu$, $F_{\mu\nu} \equiv \partial_\mu A_\nu - \partial_\nu A_\mu$ are the field strength tensors for the ω^μ , ρ and A^μ fields respectively, ∇_μ stands for covariant derivative and R is the Ricci scalar. We adopt the Lorenz gauge for the fields A_μ , ω_μ , and ρ_μ . The self-interaction scalar field potential is $U(\sigma)$, ψ_N is the nucleon isospin doublet, ψ_e is the electronic singlet, m_i states for the mass of each particle-specie and $D_\mu = \partial_\mu + \Gamma_\mu$, being Γ_μ the Dirac spin connections. The conserved currents are $J_\omega^\mu = \bar{\psi}_N\gamma^\mu\psi_N$, $J_\rho^\mu = \bar{\psi}_N\tau_3\gamma^\mu\psi_N$, $J_{\gamma,e}^\mu = \bar{\psi}_e\gamma^\mu\psi_e$, and $J_{\gamma,N}^\mu = \bar{\psi}_N(1/2)(1 + \tau_3)\gamma^\mu\psi_N$, being τ_3 the particle isospin.

The nuclear model is fixed once the values of the coupling constants and the masses of the three mesons are fixed: for instance in the NL3 parameter set Lalazissis et al. (1997) used in (Belvedere et al., 2012) and in this work we have $m_\sigma = 508.194$ MeV, $m_\omega = 782.501$ MeV, $m_\rho = 763.000$ MeV, $g_\sigma = 10.2170$, $g_\omega = 12.8680$, $g_\rho = 4.4740$, plus two constants that give the strength of the self-scalar interactions, $g_2 = -10.4310$ fm $^{-1}$ and $g_3 = -28.8850$.

From the equations of motion of the above Lagrangian we obtain the EMTF equations (see Rueda et al., 2011; Belvedere et al., 2012, for details). The solution of the EMTF coupled differential equations leads to a new structure of the star, as shown in Fig 1: a positively charged core at supranuclear densities, $\rho > \rho_{\text{nuc}} \sim 2.7 \times 10^{14}$ g cm $^{-3}$, surrounded by an electron distribution of thickness $\gtrsim \hbar/(m_e c)$ and, at lower densities $\rho < \rho_{\text{nuc}}$, a neutral ordinary crust.

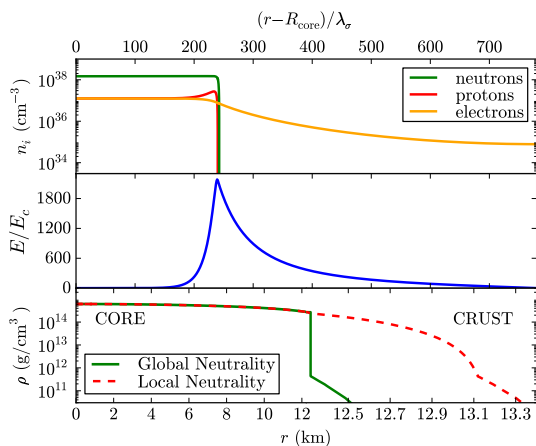


Figure 1: In the top and center panels we show the neutron, proton, electron densities and the electric field in units of the critical electric field E_c in the core-crust transition layer, whereas in the bottom panel we show a specific example of a density profile inside a neutron star. In this plot we have used for the globally neutral case a density at the edge of the crust equal to the neutron drip density, $\rho_{\text{drip}} \sim 4.3 \times 10^{11}$ g cm $^{-3}$.

The thermodynamic equilibrium is ensured by the constancy of the particle Klein potentials Klein (1949) generalized to the presence of electrostatic and strong fields (Rotondo et al., 2011; Rueda et al., 2011; Belvedere et al.,

2012)

$$\frac{1}{u^t} [\mu_i + (q_i A_\alpha + g_\omega \omega_\alpha + g_\rho \tau_{3,i} \rho_\alpha) u^\alpha] = \text{constant}, \quad (3)$$

where the subscript i stands for each kind of particle, μ_i is the particle chemical potential, and q_i is the particle electric charge. In the static case only the time components of the vector fields, A_0 , ω_0 , ρ_0 are present. In the above equation $u^t = (g_{tt})^{-1/2}$ is the time component of the fluid four-velocity which satisfies $u_\alpha u^\alpha = 1$; g_{tt} is the t-t component of the spherically symmetric metric

$$ds^2 = e^\nu dt^2 - e^\lambda dr^2 - dr^2 - r^2(d\theta^2 + \sin^2\theta d\phi^2). \quad (4)$$

The equilibrium conditions (3) lead to a discontinuity in the density at the core-crust transition and, correspondingly, an overcritical electric field $\sim (m_\pi/m_e)^2 E_c$, where $E_c = m_e^2 c^3 / (e\hbar) \sim 1.3 \times 10^{16}$ Volt cm $^{-1}$, appears in the core-crust boundary interface. The constancy of the Klein potentials is necessary to fulfill the requirement of thermodynamical equilibrium, together with the constancy of the gravitationally red-shifted temperature (Tolman condition) (Tolman, 1930; Klein, 1949), if finite temperatures are considered (see e.g. Rueda et al., 2011). In particular, the continuity of the electron Klein potential leads to a decreasing of the electron chemical potential μ_e and density at the core-crust boundary interface. They reach values $\mu_e^{\text{crust}} < \mu_e^{\text{core}}$ and $\rho_{\text{crust}} < \rho_{\text{core}}$ at the base of the crust, where global charge neutrality is achieved.

As we showed in (Belvedere et al., 2012), the solution of this new set of equilibrium equations leads to a more compact neutron star with a less massive and thinner crust. Consequently, it leads to a new mass-radius relation which markedly differs from the one given by the solution of the TOV equations in the case of local charge neutrality; see Fig. 2.

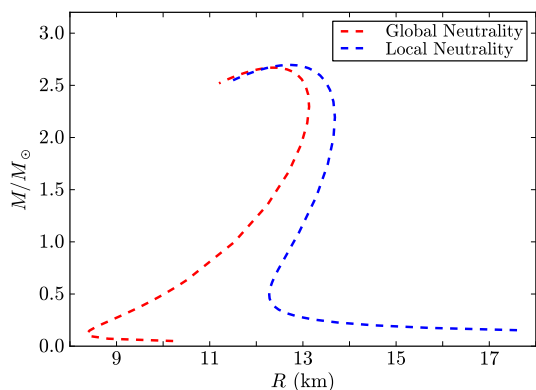


Figure 2: Neutron star mass-radius relation in the static (non-rotating) case for both global and local charge neutrality configurations (see Belvedere et al., 2012, for details). In this plot we have used for the globally neutral case a density at the edge of the crust equal to the neutron drip density, $\rho_{\text{drip}} \sim 4.3 \times 10^{11}$ g cm $^{-3}$.

We extend in this work the previous results to the case when the neutron star is rotating as a rigid body. To

this end we use the Hartle approach (Hartle, 1967) which solves the Einstein equations accurately up to second order approximation in the angular velocity of the star, Ω (see next section 2 for details).

In this rotating case, the condition of the constancy of the particle Klein potential has the same form as Eq. (3), but the fluid inside the star now moves with a four-velocity of a rigid rotating body, $u^\alpha = (u^t, 0, 0, u^\phi)$, with (see Hartle and Sharp (1967) and Appendix A, for details)

$$u^t = (g_{tt} + 2\Omega g_{t\phi} + \Omega^2 g_{\phi\phi})^{-1/2}, \quad u^\phi = \Omega u^t, \quad (5)$$

where ϕ is the azimuthal angular coordinate with respect to which the metric is symmetric, namely the metric is independent of ϕ (axial symmetry). The metric functions $g_{\alpha\beta}$ are now given by Eq. (6) below. It is then clear that in a frame comoving with the rotating star, $u^t = (g_{tt})^{-1/2}$, and the Klein equilibrium condition becomes the same as Eq. (3), as expected.

We applied the Hartle formalism to the seed static solution obtained from the integration of the EMTF equations (Belvedere et al., 2012). For the construction of the new mass-radius relation we take into account the Keplerian mass-shedding limit and the secular axisymmetric instability (see section 3). We compute in section 4 the mass M , polar R_p and equatorial R_{eq} radii, and angular momentum J , as a function of the central density and the rotation angular velocity Ω of stable neutron stars both in the globally and locally neutral cases. Based on the criteria of equilibrium we calculate the maximum stable neutron star mass and from the gravitational binding energy of the configurations establish the minimum mass under which the neutron star becomes gravitationally unbound. We construct in section 5 the new neutron star mass-radius relation. In section 6 we calculate the moment of inertia as a function of the central density and total mass of the neutron star. The eccentricity ϵ , the rotational to gravitational energy ratio T/W , and quadrupole moment Q are shown in section 7. The observational constraints on the mass-radius relation are discussed in section 8. We finally summarize the results in section 9.

2. Hartle slow rotation approximation

In his pioneering work, Hartle (1967) computed the equilibrium equations of slowly rotating stars in the context of General Relativity. The solutions of the Einstein equations are obtained through a perturbative method, expanding the metric functions up to the second order in the angular velocity Ω . Under this assumption the structure of compact objects can be approximately described by the total mass M , angular momentum J and quadrupole moment Q . The slow rotation regime implies that the perturbations owing to the rotation are relatively small with respect to the known non-rotating geometry. The interior solution is derived by solving numerically a system of ordinary differential equations for the perturbation functions.

The exterior solution for the vacuum surrounding the star, can be written analytically in terms of M , J , and Q (see Hartle, 1967; Hartle and Thorne, 1968, for details). The numerical values for all the physical quantities are derived by matching the interior and the exterior solution on the border of the star.

The spacetime metric for the rotating configuration up to the second order of Ω is given by (Hartle, 1967)

$$ds^2 = e^\nu (1 + 2h) dt^2 - e^\lambda \left[1 + \frac{2m}{r - 2M_0} \right] dr^2 - r^2 (1 + 2k) \left[d\theta^2 + \sin^2 \theta (d\phi - \omega dt)^2 \right], \quad (6)$$

where $\nu = \nu(r)$, $\lambda = \lambda(r)$, and $M_0 = M^{J=0}(r)$ are the metric functions and mass profiles of the corresponding seed non-rotating star with the same central density as the rotating one; see Eq. (4). The functions $h = h(r, \theta)$, $m = m(r, \theta)$, $k = k(r, \theta)$ and the fluid angular velocity in the local inertial frame, $\omega = \omega(r)$, have to be calculated from the Einstein equations. Expanding up to the second order the metric in spherical harmonics we have

$$h(r, \theta) = h_0(r) + h_2(r)P_2(\cos \theta), \quad (7)$$

$$m(r, \theta) = m_0(r) + m_2(r)P_2(\cos \theta), \quad (8)$$

$$k(r, \theta) = k_0(r) + k_2(r)P_2(\cos \theta), \quad (9)$$

where $P_2(\cos \theta)$ is the Legendre polynomial of second order. Because the metric does not change under transformations of the type $r \rightarrow f(r)$, we can assume $k_0(r) = 0$.

The functions $h = h(r, \theta)$, $m = m(r, \theta)$, $k = k(r, \theta)$ have analytic form in the exterior (vacuum) spacetime and they can be found in Appendix A. The mass, angular momentum, and quadrupole moment are computed from the matching condition between the interior and exterior metrics.

First the angular momentum is computed. It is introduced the angular velocity of the fluid relative to the local inertial frame, $\bar{\omega}(r) = \Omega - \omega(r)$. It can be shown from the Einstein equations at first order in Ω that $\bar{\omega}$ satisfies the differential equation

$$\frac{1}{r^4} \frac{d}{dr} \left(r^4 j \frac{d\bar{\omega}}{dr} \right) + \frac{4}{r} \frac{dj}{dr} \bar{\omega} = 0, \quad (10)$$

where $j(r) = e^{-(\nu+\lambda)/2}$ with ν and λ the metric functions of the seed non-rotating solution (4).

From the matching equations, the angular momentum of the star results to be given by

$$J = \frac{1}{6} R^4 \left(\frac{d\bar{\omega}}{dr} \right)_{r=R}, \quad (11)$$

so the angular velocity Ω is related to the angular momentum as

$$\Omega = \bar{\omega}(R) + \frac{2J}{R^3}. \quad (12)$$

The total mass of the rotating star, M , is given by

$$M = M_0 + \delta M, \quad \delta M = m_0(R) + J^2/R^3, \quad (13)$$

where δM is the contribution to the mass owing to rotation. The second order functions m_0 and p_0^* (related to the pressure perturbation) are computed from the solution of the differential equation

$$\frac{dm_0}{dr} = 4\pi r^2 \frac{d\mathcal{E}}{dP} (\mathcal{E} + P) p_0^* + \frac{1}{12} j^2 r^4 \left(\frac{d\bar{\omega}}{dr} \right)^2 - \frac{1}{3} \frac{dj^2}{dr} r^3 \bar{\omega}^2, \quad (14)$$

$$\frac{dp_0^*}{dr} = -\frac{m_0(1 + 8\pi r^2 P)}{(r - 2M_0)^2} - \frac{4\pi r^2 (\mathcal{E} + P)}{(r - 2M_0)} p_0^* + \frac{1}{12} \frac{j^2 r^4}{(r - 2M_0)} \left(\frac{d\bar{\omega}}{dr} \right)^2 + \frac{1}{3} \frac{d}{dr} \left(\frac{r^3 j^2 \bar{\omega}^2}{r - 2M_0} \right), \quad (15)$$

where \mathcal{E} and P are the total energy-density and pressure.

Turning to the quadrupole moment of the neutron star, it is given by

$$Q = \frac{J^2}{M_0} + \frac{8}{5} \mathcal{K} M_0^3, \quad (16)$$

where \mathcal{K} is a constant of integration. This constant is fixed from the matching of the second order function h_2 obtained in the interior from

$$\frac{dk_2}{dr} = -\frac{dh_2}{dr} - h_2 \frac{d\nu}{dr} + \left(\frac{1}{r} + \frac{1}{2} \frac{d\nu}{dr} \right) \left[-\frac{1}{3} r^3 \bar{\omega}^2 \frac{dj^2}{dr} + \frac{1}{6} r^4 j^2 \left(\frac{d\bar{\omega}}{dr} \right)^2 \right], \quad (17)$$

$$\begin{aligned} \frac{dh_2}{dr} = & h_2 \left\{ -\frac{d\nu}{dr} + \frac{r}{r - 2M_0} \left(\frac{d\nu}{dr} \right)^{-1} \left[8\pi (\mathcal{E} + P) - \frac{4M_0}{r^3} \right] \right\} - \frac{4(k_2 + h_2)}{r(r - 2M_0)} \left(\frac{d\nu}{dr} \right)^{-1} \\ & + \frac{1}{6} \left[\frac{r}{2} \frac{d\nu}{dr} - \frac{1}{r - 2M_0} \left(\frac{d\nu}{dr} \right)^{-1} \right] r^3 j^2 \left(\frac{d\bar{\omega}}{dr} \right)^2 \\ & - \frac{1}{3} \left[\frac{r}{2} \frac{d\nu}{dr} + \frac{1}{r - 2M_0} \left(\frac{d\nu}{dr} \right)^{-1} \right] r^2 \bar{\omega}^2 \frac{dj^2}{dr}, \quad (18) \end{aligned}$$

with its exterior counterpart (see Hartle (1967) and Appendix A).

It is worth to underline that the influence of the induced magnetic field owing to the rotation of the charged core of the neutron star in the globally neutral case is negligible (Boshkayev et al., 2012b). In fact, for a rotating neutron star of period $P = 10$ ms and radius $R \sim 10$ km, the radial component of the magnetic field B_r in the core interior reaches its maximum at the poles with a value $B_r \sim 2.9 \times 10^{-16} B_c$, where $B_c = m_e^2 c^3 / (e\hbar) \approx 4.4 \times 10^{13}$ G is the critical magnetic field for vacuum polarization. The angular component of the magnetic field B_θ , instead, has its maximum value at the equator and, as for the radial component, it is very low in the interior of the neutron star core, i.e. $|B_\theta| \sim 2.9 \times 10^{-16} B_c$. In the case of a sharp core-crust transition as the one studied by Belvedere et al. (2012) and shown in Fig. 1, this component will grow in the transition layer to values of the order of $|B_\theta| \sim 10^2 B_c$

(see Boshkayev et al., 2012b, for further details). However, since we are here interested in the macroscopic properties of the neutron star, we can ignore at first approximation the presence of electromagnetic fields in the macroscopic regions where they are indeed very small, and safely apply the original Hartle formulation without any generalization.

3. Stability of uniformly rotating neutron stars

3.1. Secular axisymmetric instability

In a sequence of increasing central density in the M - ρ_c curve, $\rho_c \equiv \rho(0)$, the maximum mass of a non-rotating neutron star is defined as the first maximum of such a curve, namely the point where $\partial M / \partial \rho_c = 0$. This derivative defines the secular instability point, and, if the perturbation obeys the same equation of state (EOS) as the equilibrium configuration, it coincides also with the dynamical instability point (see e.g. Shapiro and Teukolsky, 1983). In the rotating case, the situation becomes more complicated and in order to find the axisymmetric dynamical instability points, the perturbed solutions with zero frequency modes (the so-called neutral frequency line) have to be calculated. Friedman et al. (1988) however, following the works of Sorkin (1981, 1982), described a turning-point method to obtain the points at which secular instability is reached by uniformly rotating stars. In a constant angular momentum sequence, the turning point is located in the maximum of the mass-central density relation, namely the onset of secular axisymmetric instability is given by

$$\left[\frac{\partial M(\rho_c, J)}{\partial \rho_c} \right]_{J=\text{constant}} = 0, \quad (19)$$

and once the secular instability sets in, the star evolves quasi-stationarily until it reaches a point of dynamical instability where gravitational collapse sets in (Stergioulas, 2003).

The above equation defines an upper limit for the mass at a given J for a uniformly rotating star, however this criterion is a sufficient but not necessary condition for the instability. This means that all the configurations with the given angular momentum J on the right side of the turning point defined by Eq. (19) are secularly unstable, but it does not imply that the configurations on the left side of it are stable. An example of dynamically unstable configurations on the left side of the turning-point limiting boundary in neutron stars was recently shown in (Takami et al., 2011), for a specific EOS.

3.2. Keplerian mass-shedding instability

The maximum velocity for a particle to remain in equilibrium on the equator of a star, kept bound by the balance between gravitational and centrifugal force, is the Keplerian velocity of a free particle computed at the same location. As shown, for instance in (Stergioulas, 2003), a star rotating at Keplerian rate becomes unstable due to

the loss of mass from its surface. The mass shedding limiting angular velocity of a rotating star is the Keplerian angular velocity evaluated at the equator, $r = R_{\text{eq}}$, i.e. $\Omega_K^{J \neq 0} = \Omega_K(r = R_{\text{eq}})$. Friedman et al. (1986) introduced a method to obtain the maximum possible angular velocity of the star before reaching the mass-shedding limit; however Torok et al. (2008) and Bini et al. (2013), showed a simpler way to compute the Keplerian angular velocity of a rotating star. They showed that the mass-shedding angular velocity, $\Omega_K^{J \neq 0}$, can be computed as the orbital angular velocity of a test particle in the external field of the star and corotating with it on its equatorial plane at the distance $r = R_{\text{eq}}$. For the Hartle external solution, this is given by

$$\Omega_K^{J \neq 0}(r) = \sqrt{\frac{M}{r^3}} [1 - jF_1(r) + j^2F_2(r) + qF_3(r)] , \quad (20)$$

where $j = J/M^2$ and $q = Q/M^3$ are the dimensionless angular momentum and quadrupole moment. Further details and the analytical expression of the functions F_i can be found in Appendix A.

3.3. Gravitational binding energy

Besides the above stability requirements, one should check if the neutron star is gravitationally bound. In the non-rotating case, the binding energy of the star can be computed as

$$W_{J=0} = M_0 - M_{\text{rest}}^0 , \quad M_{\text{rest}}^0 = m_b A_{J=0} , \quad (21)$$

where M_{rest}^0 is the rest-mass of the star, m_b is the rest-mass per baryon, and $A_{J=0}$ is the total number of baryons inside the star. So the non-rotating star is considered bound if $W_{J=0} < 0$.

In the slow rotation approximation the total binding energy is given by (Hartle and Thorne, 1968)

$$W_{J \neq 0} = W_{J=0} + \delta W , \quad \delta W = \frac{J^2}{R^3} - \int_0^R 4\pi r^2 B(r) dr , \quad (22)$$

where

$$B(r) = (\mathcal{E} + P)p_0^* \left\{ \frac{d\mathcal{E}}{dP} \left[\left(1 - \frac{2M}{r}\right)^{-1/2} - 1 \right] - \frac{du}{dP} \left(1 - \frac{2M}{r}\right)^{-1/2} \right\} + (\mathcal{E} - u) \left(1 - \frac{2M}{r}\right)^{-3/2} \left[\frac{m_0}{r} + \frac{1}{3} j^2 r^2 \bar{\omega}^2 \right] - \frac{1}{4\pi r^2} \left[\frac{1}{12} j^2 r^4 \left(\frac{d\bar{\omega}}{dr}\right)^2 - \frac{1}{3} \frac{dj^2}{dr} r^3 \bar{\omega}^2 \right] , \quad (23)$$

where $u = \mathcal{E} - m_b n_b$ is the internal energy of the star, with n_b the baryon number density.

We will therefore request that the binding energy be negative, namely $W_{J \neq 0} < 0$. As we will show below in section 4.2.2, this condition leads to a minimum mass for the neutron star under which the star becomes gravitationally unbound.

4. Structure of uniformly rotating neutron stars

We show now the results of the integration of the Hartle equations for the globally and locally charge neutrality neutron stars; see e.g. Fig. 1. Following Belvedere et al. (2012), we adopt, as an example, globally neutral neutron stars with a density at the edge of the crust equal to the neutron drip density, $\rho_{\text{crust}} = \rho_{\text{drip}} \approx 4.3 \times 10^{11} \text{ g cm}^{-3}$.

4.1. Secular instability boundary

In Fig. 3 we show the mass-central density curve for globally neutral neutron stars in the region close to the axisymmetric stability boundaries. Specifically we show some J -constant sequences to show that indeed along each of these curves there exist a maximum mass point (turning point). The line joining all the turning points defines the secular instability limit. In Fig. 3 the axisymmetric stable zone is on the left side of the instability line.

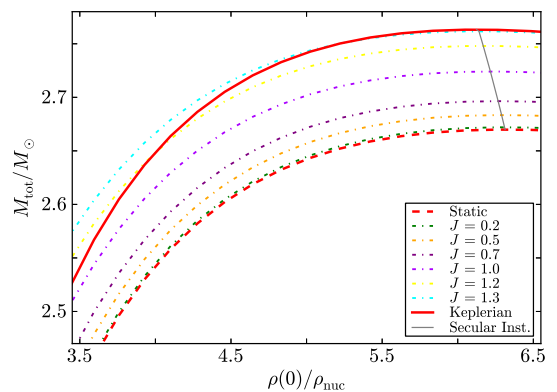


Figure 3: Total mass versus central density of globally neutral neutron stars. The solid line represents the configuration with Keplerian angular velocity, the dashed line represents the static configuration, the dotted-dashed lines represent the J -constant sequences (in units of 10^{11} cm^2). The gray line joins all the turning points of the J -constant sequences, so it defines the secular instability boundary.

Clearly we can transform the mass-central density relation in a mass-radius relation. In Fig. 4 we show the mass versus the equatorial radius of the neutron star that correspond to the range of densities of Fig. 3. In this plot the stable zone is on the right side of the instability line.

We can construct a fitting curve joining the turning points of the J -constant sequences line which determines the secular axisymmetric instability boundary. Defining $M_{\text{max},0}$ as the maximum stable mass of the non-rotating neutron star constructed with the same EOS, we find that for globally neutral configurations the instability line is well fitted by the function

$$\frac{M_{\text{sec}}^{\text{GCN}}}{M_{\odot}} = 21.22 - 6.68 \frac{M_{\text{max},0}^{\text{GCN}}}{M_{\odot}} - \left(77.42 - 28 \frac{M_{\text{max},0}^{\text{GCN}}}{M_{\odot}} \right) \left(\frac{R_{\text{eq}}}{10 \text{ km}} \right)^{-6.08} , \quad (24)$$

where $12.38 \text{ km} \lesssim R_{\text{eq}} \lesssim 12.66 \text{ km}$, and $M_{\text{max},0}^{\text{GCN}} \approx 2.67 M_{\odot}$.

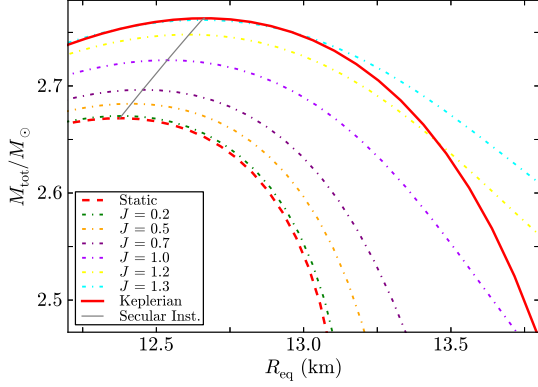


Figure 4: Total mass versus equatorial radius of globally neutral neutron stars. The solid line represents the configuration with Keplerian angular velocity, the dashed line represents the static configuration, the dotted-dashed lines represent the J -constant sequences (in units of 10^{11} cm^2). The gray curve joins all the turning points of the J -constant sequences, so it defines the secular instability boundary.

The turning points of locally neutral configurations in the mass-central density plane are shown in Fig. 5. the corresponding mass-equatorial radius plane is plotted in Fig. 6.

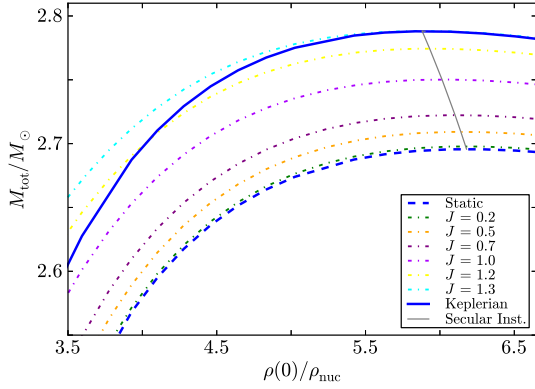


Figure 5: Total mass versus central density of locally neutral neutron stars. The solid line represents the configuration with Keplerian angular velocity, the dashed line represents the static configuration, the dotted-dashed lines represent the J -constant sequences (in units of 10^{11} cm^2). The gray line joins all the turning points of the J -constant sequences, so it defines the secular instability boundary.

For locally neutral neutron stars, the secular instability line is fitted by

$$\frac{M_{\text{sec}}^{\text{LCN}}}{M_{\odot}} = 20.51 - 6.35 \frac{M_{\text{max},0}^{\text{LCN}}}{M_{\odot}} - \left(80.98 - 29.02 \frac{M_{\text{max},0}^{\text{LCN}}}{M_{\odot}} \right) \left(\frac{R_{\text{eq}}}{10 \text{ km}} \right)^{-5.71}, \quad (25)$$

where $12.71 \text{ km} \lesssim R_{\text{eq}} \lesssim 13.06 \text{ km}$, and $M_{\text{max},0}^{\text{LCN}} \approx 2.70 M_{\odot}$.

4.2. Keplerian mass-shedding sequence

We turn now to analyze in detail the behavior of the different properties of the neutron star along the Keple-

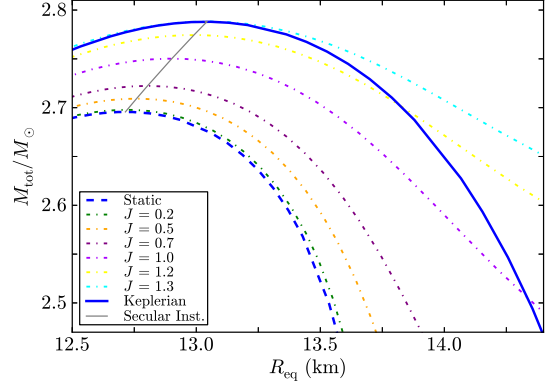


Figure 6: Total mass versus equatorial radius of locally neutral neutron stars. The solid line represents the configuration with Keplerian angular velocity, the dashed line represents the static configuration, the dotted-dashed lines represent the J -constant sequences (in units of 10^{11} cm^2). The gray curve joins all the turning points of the J -constant sequences, so it defines the secular instability boundary.

rian mass-shedding sequence. For the sake of reference we have indicated in the following plots stars with the selected masses $M \approx [1, 1.4, 2.04, 2.5] M_{\odot}$. The cyan star indicates the fastest observed pulsar, PSR J1748–2446ad Hessels et al. (2006), with a rotation frequency of $f \approx 716 \text{ Hz}$. The gray filled circles indicate the last stable configuration of the Keplerian sequence, namely the point where the Keplerian and the secular stability boundaries cross each other.

4.2.1. Maximum mass and rotation frequency

The total mass of the rotating star is computed from Eq. (13). In Fig. 7 is shown the total mass of the neutron star as a function of the rotation frequency for the Keplerian sequence. It is clear that for a given mass, the rotational frequency is higher for a globally neutral neutron star with respect to the locally neutral one.

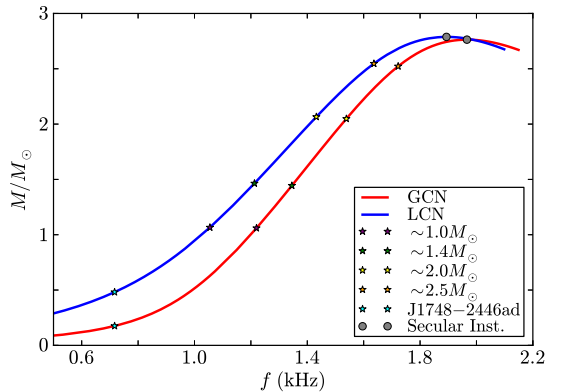


Figure 7: Total mass versus rotational Keplerian frequency both for the global (red) and local (blue) charge neutrality cases.

The configuration of maximum mass, $M_{\text{max}}^{J \neq 0}$, occurs along the Keplerian sequence, and it is found before the secular instability line crosses the Keplerian curve. Thus,

the maximum mass configuration is secularly stable. This implies that the configuration with maximum rotation frequency, f_{\max} , is located beyond the maximum mass point, specifically at the crossing point between the secular instability and the Keplerian mass-shedding sequence. The results are summarized in Table 1.

It is important to discuss briefly the validity of the present perturbative solution for the computation of the properties of maximally rotating neutron stars. The expansion of the radial coordinate of a rotating configuration $r(R, \theta)$ in powers of angular velocity is written as (Hartle, 1967)

$$r = R + \xi(R, \theta) + O(\Omega^4), \quad (26)$$

where ξ is the difference in the radial coordinate, r , between a point located at the polar angle θ on the surface of constant density $\rho(R)$ in the rotating configuration, and the point located at the same polar angle on the same constant density surface in the non-rotating configuration. In the slow rotation regime, the fractional displacement of the surfaces of constant density due to the rotation have to be small, namely $\xi(R, \theta)/R \ll 1$, where $\xi(R, \theta) = \xi_0(R) + \xi_2(R)P_2(\cos \theta)$ and $\xi_0(R)$ and $\xi_2(R)$ are function of R , proportional to Ω^2 . From Table 1, we can see that the configuration with the maximum possible rotation frequency has a maximum fractional displacement $\delta R_{\text{eq}}^{\max} = \xi(R, \pi/2)/R$ as low as $\approx 2\%$ and $\approx 3\%$, for the globally and locally neutral neutron stars respectively.

In this line, it is worth to quote the results of Benhar et al. (2005), who showed that the inclusion of a third-order expansion Ω^3 in the Hartle's method improves the value of the maximum rotation frequency by less than 1% for different EOS. The reason for this is that as mentioned above, along the Keplerian sequence the deviations from sphericity decrease with density and frequency (see Figs. 16 and 17), which ensures the accuracy of the perturbative solution.

Turning to the increase of the maximum mass, Weber and Glendenning (1992) showed that the mass of maximally rotating neutron stars, computed with the Hartle's second order approximation, is accurate within an error as low as $\lesssim 4\%$.

4.2.2. Minimum mass and rotation frequency

We compute now the gravitational binding energy of the neutron star from Eq. (22) as a function of the central density and angular velocity. We make this for central densities higher than the nuclear density, thus we impose the neutron star to have a supranuclear hadronic core. In Fig. 8 we plot the binding energy W of the neutron star as a function of the neutron star mass along the Keplerian sequence. For the sake of comparison we show also the binding energy of the non-rotating configurations.

We found that the globally neutral neutron stars studied here are bound up to some minimum mass at which the gravitational binding energy vanishes. For the static and Keplerian configurations we find that $W_{J=0} = 0$, and

	Global Neutrality	Local Neutrality
$M_{\max}^{J=0}$ (M_{\odot})	2.67	2.70
$R_{\max}^{J=0}$ (km)	12.38	12.71
$M_{\max}^{J \neq 0}$ (M_{\odot})	2.76	2.79
$R_{\max}^{J \neq 0}$ (km)	12.66	13.06
δM_{\max}	3.37%	3.33%
$\delta R_{\text{eq}}^{\max}$	2.26%	2.75%
f_{\max} (kHz)	1.97	1.89
P_{\min} (ms)	0.51	0.53

Table 1: $M_{\max}^{J=0}$ and $R_{\max}^{J=0}$: maximum mass and corresponding radius of non-rotating stars as computed in (Belvedere et al., 2012); $M_{\max}^{J \neq 0}$ and $R_{\max}^{J \neq 0}$: maximum mass and corresponding radius of rotating stars; δM_{\max} and $\delta R_{\text{eq}}^{\max}$: increase in mass and radius of the maximum mass configuration with respect to its non-rotating counterpart; f_{\max} and P_{\min} : maximum rotation frequency and associated minimum period.

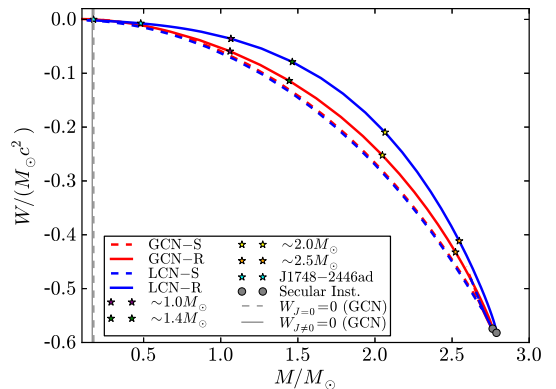


Figure 8: Neutron star binding energy versus total mass along the Keplerian sequence both for the global (red) and local (blue) charge neutrality.

$W_{J \neq 0} = 0$ respectively at

$$M_{\min}^{J=0} \approx 0.177 M_{\odot}, \quad M_{\min}^K \approx 0.167 M_{\odot}, \quad (27)$$

where with the superscript K we indicate that this value corresponds to the minimum mass on the Keplerian sequence. Clearly this minimum mass value decreases with decreasing frequency until it reaches the above value $M_{\min}^{J=0}$ of the non-rotating case.

We did not find any unbound configuration in the local charge neutrality case for the present EOS (see Fig. 8). The corresponding plot of W as a function of the central density is shown in Fig. 9.

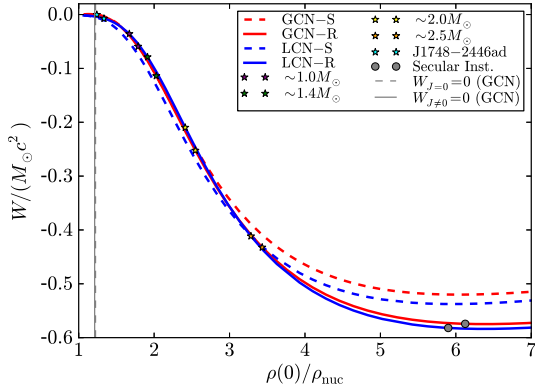


Figure 9: Neutron star binding energy versus central density along the Keplerian sequence both for the global (red) and local (blue) charge neutrality.

The configuration with the minimum mass, $M_{\min}^K \approx 0.167 M_{\odot}$, has a rotation frequency

$$f_{\min}^K = f(M_{\min}^K) \approx 700.59 \text{ Hz}, \quad (28)$$

that is the minimum rotation rate that globally neutral configurations can have along the Keplerian sequence in order to be gravitationally bound. Interestingly, the above value is slightly lower than the frequency of the fastest observed pulsar, PSR J1748–2446ad, which has a frequency of 716 Hz Hessels et al. (2006). Further discussions on this issue are given below in section 8.

In Fig. 10 we show in detail the dependence of W on the rotation frequency.

5. Neutron star mass-radius relation

We summarize now the above results in form of a new mass-radius relation of uniformly rotating neutron stars, including the Keplerian and secular instability boundary limits. In Fig. 11 we show a summary plot of the equilibrium configurations of rotating neutron stars. In particular we show the total mass versus the equatorial radius: the dashed lines represent the static (non-rotating, $J = 0$) sequences, while the solid lines represent the corresponding Keplerian mass-shedding sequences. The secular instability boundaries are plotted in pink-red and light blue color

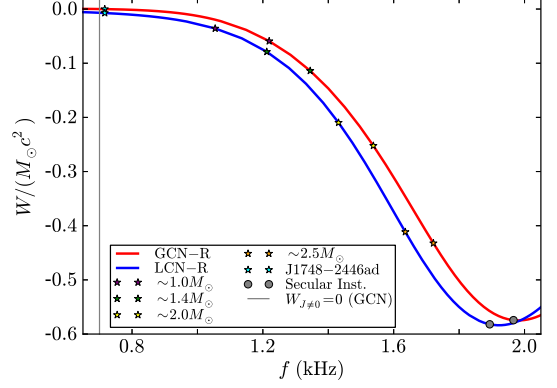


Figure 10: Neutron star binding energy versus frequency for the Keplerian sequence both for the global (red) and local (blue) charge neutrality neutron stars.

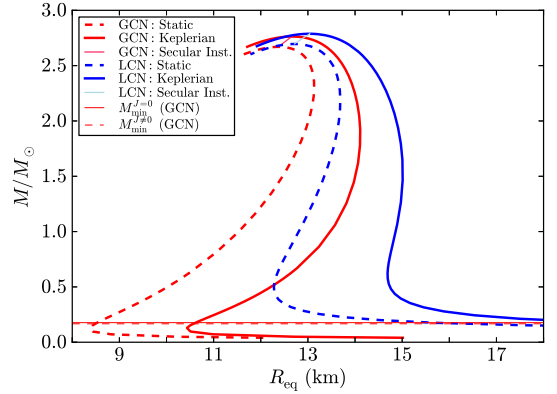


Figure 11: Total mass versus total equatorial radius for the global (red) and local (blue) charge neutrality cases. The dashed curves represent the static configurations, while the solid lines are the uniformly rotating neutron stars. The pink-red and light-blue color lines define the secular instability boundary for the globally and locally neutral cases, namely the lines given by Eqs. (24) and (25), respectively.

for the global and local charge neutrality cases, respectively.

It can be seen that due to the deformation for a given mass the radius of the rotating case is larger than the static one, and similarly the mass of the rotating star is larger than the corresponding static one. It can be also seen that the configurations obeying global charge neutrality are more compact with respect to the ones satisfying local charge neutrality.

6. Moment of inertia

The neutron star moment of inertia I can be computed from the relation

$$I = \frac{J}{\Omega}, \quad (29)$$

where J is the angular momentum and Ω are related via Eq. (12). Since J is a first-order quantity and so proportional to Ω , the moment of inertia given by Eq. (29) does not depend on the angular velocity and does not take into account deviations from the spherical symmetry. This implies that Eq. (11) gives the moment of inertia of the non-rotating unperturbed seed object. In order to find the perturbation to I , say δI , the perturbative treatment has to be extended to the next order Ω^3 , in such a way that $I = I_0 + \delta I = (J_0 + \delta J)/\Omega$, becomes of order Ω^2 , with δJ of order Ω^3 (see e.g. Hartle, 1973; Benhar et al., 2005). In this work we keep the solution up to second order and therefore we proceed to analyze the behavior of the moment of inertia for the non-rotating configurations. In any case, as we will show in section 8 even the fastest observed pulsars rotate at frequencies much lower than the Keplerian rate, and under such conditions we expect that the moment of inertia can be approximated with high accuracy by the one of the corresponding static configurations.

In Figs. 12 and 13 we show the behavior of the total momentum of inertia, i.e. $I = I_{\text{core}} + I_{\text{crust}}$, with respect to the total mass and central density for both globally and locally neutral non-rotating neutron stars.

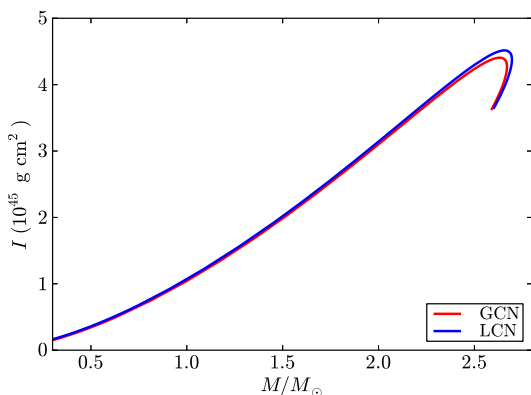


Figure 12: Total moment of inertia versus total mass both for globally (red) and locally (blue) neutral non-rotating neutron stars.

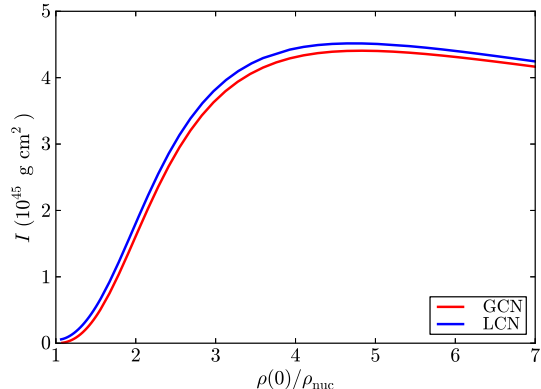


Figure 13: Total moment of inertia versus central density for globally (red) and locally (blue) neutral non-rotating neutron stars.

We can see from Figs. 12 and 13 that the total moment of inertia is quite similar for both global and local charge neutrality cases. This is due to the fact that the globally neutral configurations differ from the locally ones mostly in the structure of the crust, which however contributes much less than the neutron star core to the total moment of inertia (see below in section 6.1).

6.1. Core and crust moment of inertia

In order to study the single contribution of the core and the crust to the moment of inertia of the neutron star, we shall use the integral expression for the moment of inertia. Multiplying Eq. (10) by r^3 and making the integral of it we obtain²

$$\begin{aligned} I(r) &= -\frac{2}{3} \int_0^r r^3 \frac{dj}{dr} \frac{\bar{\omega}(r)}{\Omega} dr \\ &= \frac{8\pi}{3} \int_0^r r^4 (\mathcal{E} + P) e^{(\lambda-\nu)/2} \frac{\bar{\omega}(r)}{\Omega} dr, \end{aligned} \quad (30)$$

where the integration is carried out in the region of interest. Thus, the contribution of the core, I_{core} , is obtained integrating from the origin up to the radius of the core, and the contribution of the crust, I_{crust} , integrating from the base of the crust to the total radius of the neutron star.

We show in Figs. 14 and 15 the ratio between the moment of inertia of the crust and the one of the core as a function of the total mass and central density, respectively, for both the globally and locally neutral configurations.

7. Deformation of the neutron star

In this section we explore the deformation properties of the neutron star. The behavior of the eccentricity, the rotational to gravitational energy ratio, as well as the quadrupole moment, are investigated as a function of the mass, density, and rotation frequency of the neutron star.

²It is clear that this expression approaches, in the weak field limit, the classic Newtonian expression $I_{\text{Newtonian}} = (8\pi/3) \int r^4 \rho dr$ where ρ is the mass-density (Hartle, 1967).

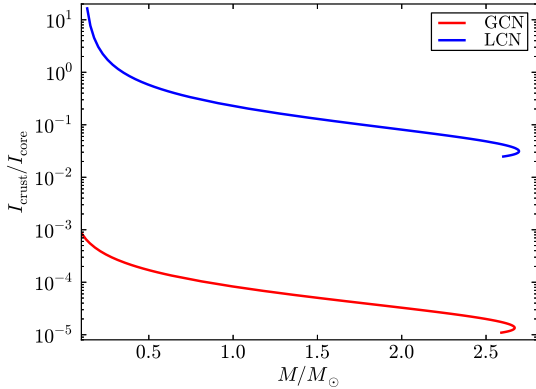


Figure 14: Crust to core moment of inertia ratio versus the total mass of both globally and locally neutral non-rotating neutron stars.

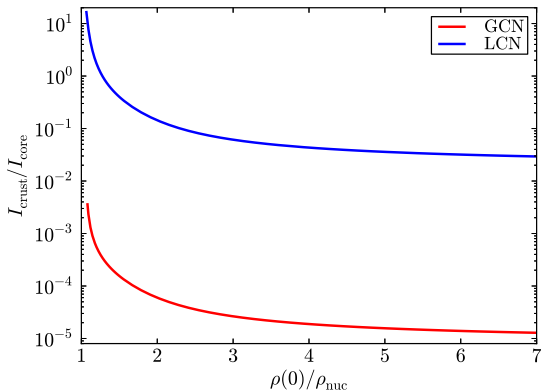


Figure 15: Crust to core moment of inertia ratio versus the central density both globally and locally neutral non-rotating neutron stars.

7.1. Eccentricity

A measurement of the level of deformation of the neutron star can be estimated with the eccentricity

$$\epsilon = \sqrt{1 - \left(\frac{R_p}{R_{\text{eq}}}\right)^2}, \quad (31)$$

where R_p and R_{eq} are the polar and equatorial radii of the configuration. Thus, $\epsilon = 0$ defines the spherical limit and $0 < \epsilon < 1$ corresponds to oblate configurations.

In Fig. 16, we show the behavior of the total eccentricity (31), as a function of the neutron star frequency.

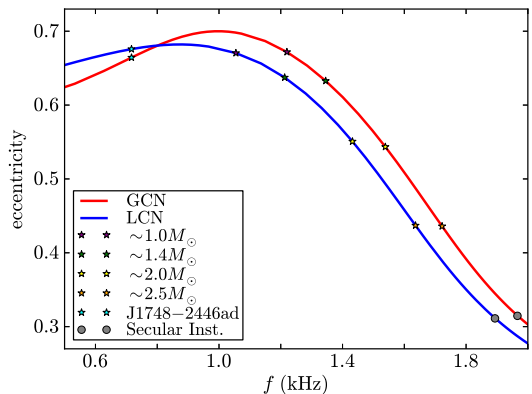


Figure 16: Eccentricity (31) versus frequency for the Keplerian sequence both for the global (red) and local (blue) charge neutrality cases.

We can see that in general the globally neutral neutron star has an eccentricity larger than the one of the locally neutral configuration for almost the entire range of frequencies and the corresponding central densities, except for the low frequencies $f \lesssim 0.8$ kHz and central densities $\rho(0) \lesssim 1.3\rho_{\text{nuc}}$; see also Fig. 17. Starting from low values of the frequency f and central density $\rho(0)$, the neutron stars increase their oblateness, and after reaching the maximum value of the eccentricity, the compactness increases and the configurations tend to a more spherical shape.

7.2. Rotational to gravitational energy ratio

Other property of the star related to the centrifugal deformation of the star is the ratio between the gravitational energy and the rotational energy of the star. The former is given by Eq. (22), whereas the latter is

$$T = \frac{1}{2}I\Omega^2, \quad (32)$$

We show in Fig. 18 the ratio $T/|W|$ as a function of the mass of the neutron stars along the Keplerian sequence. In Fig. 19 instead we plot the dependence of the ratio on the central density and in Fig. 20 on the Keplerian frequency.

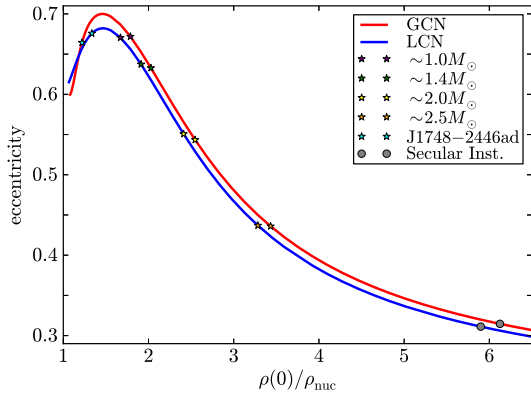


Figure 17: Eccentricity (31) versus central density for the Keplerian sequence both for the global (red) and local (blue) charge neutrality cases.

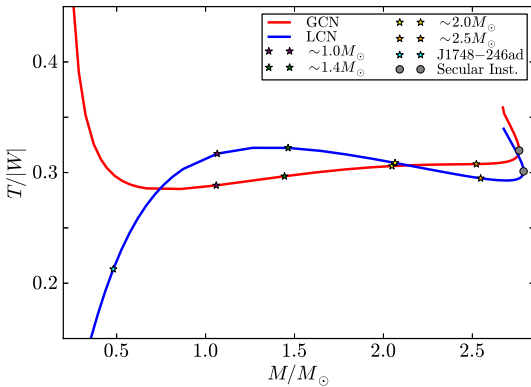


Figure 18: Rotational to gravitational binding energy ratio versus total mass along the Keplerian sequence both for the global (red) and local (blue) charge neutrality.

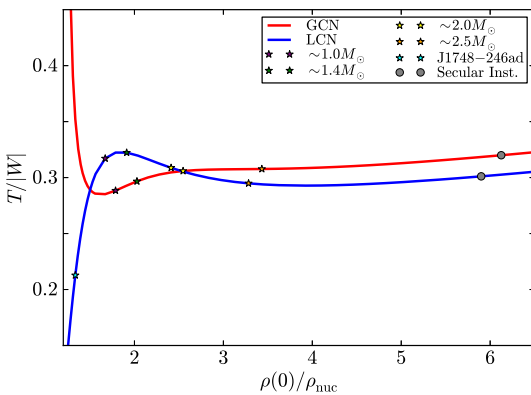


Figure 19: Rotational to gravitational binding energy ratio versus central density along the Keplerian sequence both for the global (red) and local (blue) charge neutrality.

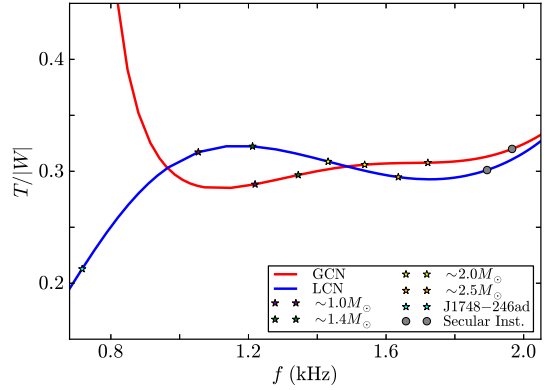


Figure 20: Rotational to gravitational binding energy ratio versus frequency along the Keplerian sequence both for the global (red) and local (blue) charge neutrality cases.

7.3. Quadrupole moment

In Figs. 21 and 22 we show the quadrupole moment, Q given by Eq. (16), as a function of the total mass and central density for both globally and locally neutral neutron stars along the Keplerian sequence. The dependence of Q on the rotation frequency is shown in Fig. 23. We have normalized the quadrupole moment Q to the quantity MR^2 of the non-rotating configuration with the same central density.

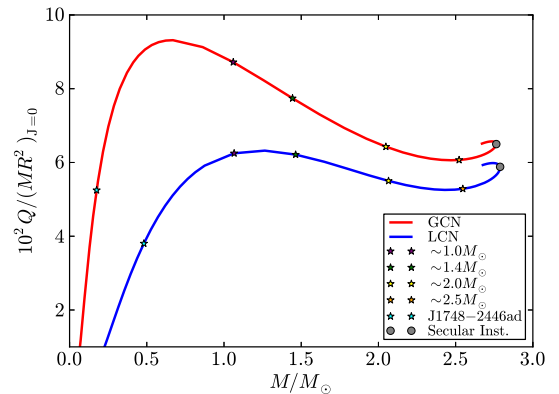


Figure 21: Total quadrupole moment versus total mass along the Keplerian sequence both for the global (red) and local (blue) charge neutrality cases. The quadrupole moment Q is here in units of the quantity MR^2 of the non-rotating configuration with the same central density.

8. Observational constraints

In Fig. 24 we show the above mass-radius relations together with the most recent and stringent constraints indicated by Trümper (2011):

1) *The largest mass.* Until 2013 it was given by the mass of the 3.15 millisecond pulsar PSR J1614-2230 $M = 1.97 \pm 0.04 M_\odot$ Demorest et al. (2010), however the recent reported mass $2.01 \pm 0.04 M_\odot$ for the neutron star in the relativistic binary PSR J0348+0432 (Antoniadis et al., 2013)

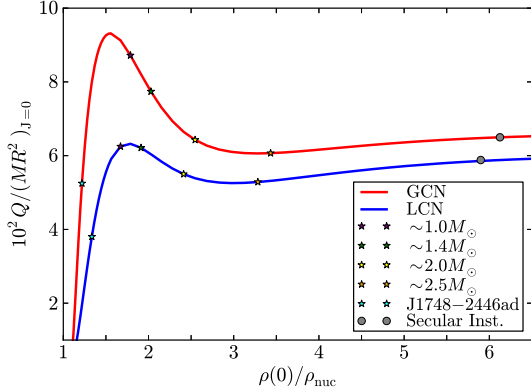


Figure 22: Total quadrupole moment versus central density along the Keplerian sequence both for the global (red) and local (blue) charge neutrality cases. The quadrupole moment Q is here in units of the quantity MR^2 of the non-rotating configuration with the same central density.

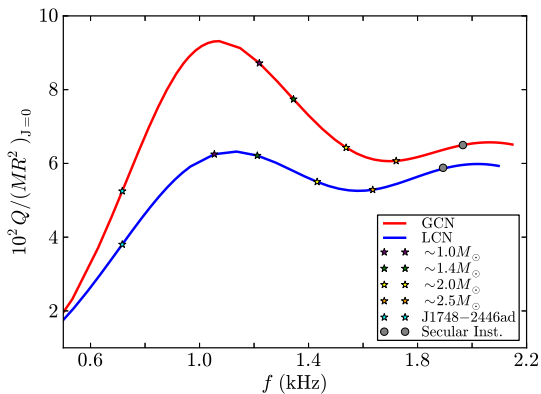


Figure 23: Total quadrupole moment versus frequency along the Keplerian sequence both for the global (red) and local (blue) charge neutrality cases. The quadrupole moment Q is here in units of the quantity MR^2 of the non-rotating configuration with the same central density.

puts an even more stringent request to the nuclear EOS. Thus, the maximum mass of the neutron star has to be larger than the mass of PSR J0348+0432, this constraint is represented by the orange-color stars in Fig. 24.

2) *The largest radius.* It is given by the lower limit to the radius of RX J1856-3754. The lower limit to the radius as seen by an observer at infinity is $R_\infty = R[1 - 2GM/(c^2R)]^{-1/2} > 16.8$ km, as given by the fit of the optical and X-ray spectra of the source Trümper et al. (2004); so in the mass-radius relation this constraint reads $2GM/c^2 > R - R^3/(R_\infty^{\min})^2$, with $R_\infty^{\min} = 16.8$ km. We represent this constraint with the dotted-dashed curve in Fig. 24.

3) *The maximum surface gravity.* Using a neutron star of $M = 1.4M_\odot$ to fit the Chandra data of the low-mass X-ray binary X7, it turns out that the radius of the star satisfies at 90% confidence level, $R = 14.5^{+1.8}_{-1.6}$ km, which gives $R_\infty = [15.64, 18.86]$ km, respectively Heinke et al. (2006). Using the same formula as before, $2GM/c^2 > R - R^3/(R_\infty^{\min})^2$, we obtain the dotted curves shown in Fig. 24.

4) *The highest rotation frequency.* The fastest observed pulsar is PSR J1748-2446ad with a frequency of 716 Hz Hessels et al. (2006). We show the constant rotation frequency sequence $f = 716$ Hz for both globally (dashed pink) and locally (dashed light blue) neutral neutron stars. We indicated with cyan-color stars the point where these curves cross the corresponding Keplerian sequences in the two cases (see Fig. 24).

Every f -constant sequence crosses the stability region of the objects in two points: these crossing points define the minimum and maximum possible mass that an object rotating with such a frequency may have in order to be stable. In the case of PSR J1748-2446ad, the cut of the $f = 716$ Hz constant sequence with the Keplerian curve establishes the minimum mass of this pulsar. We find that its minimum mass is $\approx 0.175 M_\odot$ and corresponding equatorial radius 10.61 km for the globally neutral neutron star. For the locally neutral configuration we found $\approx 0.48 M_\odot$ and 14.8 km, respectively for the minimum mass and corresponding equatorial radius. This implies that the mass of PSR J1748-2446ad is poorly constrained to be larger than the above values.

It is interesting that the above minimum mass, given by its constant rotation frequency sequence, is slightly larger than the minimum mass for bound configurations on the Keplerian sequence, $M_{\min}^K \approx 0.167 M_\odot$; see Eq. (27). In fact, as we shown in Eq. (28) the minimum rotation frequency along the Keplerian sequence for bound configurations in the globally neutral case is, $f_{\min}^K \approx 700.59$ Hz, which is slightly lower than the frequency of PSR J1748-2446ad. It would imply that PSR J1748-2446ad is very likely rotating at a rate much lower than the Keplerian one.

Similarly to what presented in Belvedere et al. (2012) for the static neutron stars and introduced by Trümper (2011), the above observational constraints show a prefer-

$M(M_\odot)$	$R^{J=0}$ (km)	$R_{\text{eq}}^{J\neq 0}$ (km)
1.40	12.313	13.943
1.97	12.991	14.104
2.01	13.020	14.097

Table 2: Radii for a canonical neutron star of $M = 1.4M_\odot$ and for PSR J1614–2230 Demorest et al. (2010), $M = 1.97 \pm 0.04M_\odot$, and PSR J0348+0432 (Antoniadis et al., 2013), $M = 2.01 \pm 0.04M_\odot$. These configurations are computed under the constraint of global charge neutrality and for a density at the edge of the crust equal to the neutron drip density. The nuclear parameterizations NL3 has been used.

ence on stiff EOS that provide highest maximum masses for neutron stars. Taking into account the above constraints, the radius of a canonical neutron star of mass $M = 1.4M_\odot$ is strongly constrained to $R \geq 12$ km, disfavoring at the same time strange quark matter stars. It is evident from Fig. 24 that mass-radius relations for both the static and the rotating case presented here, are consistent with all the observational constraints. In Table 2 we show the radii predicted by our mass-radius relation both for the static and the rotating case for a canonical neutron star as well as for the most massive neutron stars discovered, namely, the millisecond pulsar PSR J1614–2230 Demorest et al. (2010), $M = 1.97 \pm 0.04M_\odot$, and the most recent PSR J0348+0432, $M = 2.01 \pm 0.04M_\odot$ (Antoniadis et al., 2013).

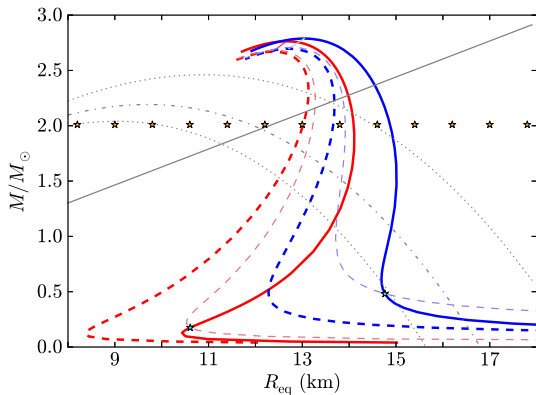


Figure 24: Observational constraints on the mass-radius relation given by Trümper (2011) and the theoretical mass-radius relation presented in this work in Fig. 11. The red lines represent the configuration with global charge neutrality, while the blue lines represent the configuration with local charge neutrality. The pink-red line and the light-blue line represent the secular axisymmetric stability boundaries for the globally neutral and the locally neutral case, respectively. The red and blue solid lines represent the Keplerian sequences and the red and blue dashed lines represent the static cases presented in (Belvedere et al., 2012).

9. Concluding remarks

We have constructed equilibrium configurations of uniformly rotating neutron stars in both the global charge neutrality and local charge neutrality cases, generalizing

	Global Neutrality	Local Neutrality
$M_{\text{max}}^{J=0}(M_\odot)$	2.67	2.70
$M_{\text{max}}^{J\neq 0}(M_\odot)$	2.76	2.79
f_{max} (kHz)	1.97	1.89
P_{min} (ms)	0.51	0.53
$M_{\text{min}}^{J=0}(M_\odot)$	0.18	–
$M_{\text{min}}^K(M_\odot)$	0.17	–
f_{min}^K (kHz)	0.70	–

Table 3: Maximum mass, maximum frequency, minimum period, minimum mass of globally and locally neutral neutron stars.

our previous work (Belvedere et al., 2012). To do this we have applied the Hartle method to the seed static solution obtained from the integration of the Einstein-Maxwell-Thomas-Fermi equations (Belvedere et al., 2012). We calculated the mass, polar and equatorial radii, angular momentum, moment of inertia, quadrupole moment, and eccentricity, as functions of the central density and the rotation angular velocity of the neutron star.

The Keplerian mass-shedding limit and the secular axisymmetric instability have been analyzed for the construction of the region of stability of rotating neutron stars. We have given fitting curves of the secular instability boundary in Eqs. (24) and (25) for global and local charge neutrality, respectively. With this analysis we have established in section 4.2.1 the maximum mass and maximum rotation frequency of the neutron star. We computed in section 4.2.2 the gravitational binding energy of the configurations as a function of the central density and rotation rate. We did this for central densities higher than the nuclear one, so imposing that the neutron star has a supranuclear hadronic core. We found that there is a minimum mass under which the neutron star becomes gravitationally unbound. Along the Keplerian sequence, to this minimum mass object we associate a minimum frequency under which an object rotating at the Keplerian rate becomes unbound; see Eq. (28). We found that locally neutral neutron stars with supranuclear cores remained always bound for the present EOS. In Table 3 we summarize all these results.

We finally analyzed in section 8 the current observational constraints on the mass-radius relation of neutron stars. We constructed the constant frequency sequence of PSR J1748–2446ad to obtain the minimum possible mass of this source, which is given by the crossing point of the $f = 716$ Hz constant sequence with the Keplerian one. It gives $\approx 0.17 M_\odot$ and $\approx 0.48 M_\odot$ for the global and charge neutrality cases, respectively. The very low mass inferred for PSR J1748–2446ad assuming that it rotates at the Keplerian rate implies that its frequency is unlikely to be actually the Keplerian. Otherwise, it would imply that PSR J1748–32446ad could be the less massive neutron star ever observed.

It would be interesting to analyze the generality of the neutron star features shown in this work since the most

recent measurement of the mass PSR J0348+0432, $M = 2.01 \pm 0.04 M_{\odot}$ (Antoniadis et al., 2013), favors stiff nuclear EOS as the one used here.

References

References

Antoniadis, J., Freire, P. C. C., Wex, N., Tauris, T. M., Lynch, R. S., van Kerkwijk, M. H., Kramer, M., Bassa, C., Dhillon, V. S., Driebe, T., Hessels, J. W. T., Kaspi, V. M., Kondratiev, V. I., Langer, N., Marsh, T. R., McLaughlin, M. A., Pennucci, T. T., Ransom, S. M., Stairs, I. H., van Leeuwen, J., Verbiest, J. P. W., Whelan, D. G., Apr. 2013. A Massive Pulsar in a Compact Relativistic Binary. *Science* 340, 448.

Belvedere, R., Pugliese, D., Rueda, J. A., Ruffini, R., Xue, S.-S., Jun. 2012. Neutron star equilibrium configurations within a fully relativistic theory with strong, weak, electromagnetic, and gravitational interactions. *Nuclear Physics A* 883, 1–24.

Benhar, O., Ferrari, V., Gualtieri, L., Marassi, S., Aug. 2005. Perturbative approach to the structure of rapidly rotating neutron stars. *Phys. Rev. D* 72 (4), 044028–+.

Berti, E., White, F., Maniopolou, A., Bruni, M., Apr. 2005. Rotating neutron stars: an invariant comparison of approximate and numerical space-time models. *MNRAS* 358, 923–938.

Bini, D., Boshkayev, K., Ruffini, R., Siutsou, I., 2013. Equatorial circular geodesics in the Hartle-Thorne spacetime. *Il Nuovo Cimento C* 36, 31.

Boguta, J., Bodmer, A. R., Dec. 1977. Relativistic calculation of nuclear matter and the nuclear surface. *Nuclear Physics A* 292, 413–428.

Boshkayev, K., Quevedo, H., Ruffini, R., Sep. 2012a. Gravitational field of compact objects in general relativity. *Phys. Rev. D* 86 (6), 064043.

Boshkayev, K., Rotondo, M., Ruffini, R., Mar. 2012b. On Magnetic Fields in Rotating Nuclear Matter Cores of Stellar Dimensions. *International Journal of Modern Physics Conference Series* 12, 58–67.

Demorest, P. B., Pennucci, T., Ransom, S. M., Roberts, M. S. E., Hessels, J. W. T., Oct. 2010. A two-solar-mass neutron star measured using Shapiro delay. *Nature* 467, 1081–1083.

Friedman, J. L., Ipser, J. R., Sorkin, R. D., Feb. 1988. Turning-point method for axisymmetric stability of rotating relativistic stars. *ApJ* 325, 722–724.

Friedman, J. L., Parker, L., Ipser, J. R., May 1986. Rapidly rotating neutron star models. *ApJ* 304, 115–139.

Haensel, P., Potekhin, A. Y., Yakovlev, D. G. (Eds.), 2007. *Neutron Stars 1: Equation of State and Structure*. Vol. 326 of *Astrophysics and Space Science Library*.

Hartle, J. B., Dec. 1967. Slowly Rotating Relativistic Stars. I. Equations of Structure. *ApJ* 150, 1005.

Hartle, J. B., Oct. 1973. Slowly Rotating Relativistic Stars. IX: Moments of Inertia of Rotationally Distorted Stars. *Ap&SS* 24, 385–405.

Hartle, J. B., Sharp, D. H., Jan. 1967. Variational Principle for the Equilibrium of a Relativistic, Rotating Star. *ApJ* 147, 317–+.

Hartle, J. B., Thorne, K. S., Sep. 1968. Slowly Rotating Relativistic Stars. II. Models for Neutron Stars and Supermassive Stars. *ApJ* 153, 807.

Heinke, C. O., Rybicki, G. B., Narayan, R., Grindlay, J. E., Jun. 2006. A Hydrogen Atmosphere Spectral Model Applied to the Neutron Star X7 in the Globular Cluster 47 Tucanae. *ApJ* 644, 1090–1103.

Hessels, J. W. T., Ransom, S. M., Stairs, I. H., Freire, P. C. C., Kaspi, V. M., Camilo, F., Mar. 2006. A Radio Pulsar Spinning at 716 Hz. *Science* 311, 1901–1904.

Klein, O., Jul. 1949. On the Thermodynamical Equilibrium of Fluids in Gravitational Fields. *Reviews of Modern Physics* 21, 531–533.

Lalazissis, G. A., König, J., Ring, P., Jan. 1997. New parametrization for the Lagrangian density of relativistic mean field theory. *Phys. Rev. C* 55, 540–543.

Oppenheimer, J. R., Volkoff, G. M., Feb. 1939. On Massive Neutron Cores. *Phys. Rev.* 55, 374–381.

Rotondo, M., Rueda, J. A., Ruffini, R., Xue, S.-S., Jul. 2011. The self-consistent general relativistic solution for a system of degenerate neutrons, protons and electrons in β -equilibrium. *Physics Letters B* 701, 667–671.

Rueda, J. A., Ruffini, R., Xue, S.-S., Dec. 2011. The Klein first integrals in an equilibrium system with electromagnetic, weak, strong and gravitational interactions. *Nuclear Physics A* 872, 286–295.

Shapiro, S. L., Teukolsky, S. A., 1983. *Black holes, white dwarfs, and neutron stars: The physics of compact objects*.

Sorkin, R., Oct. 1981. A Criterion for the Onset of Instability at a Turning Point. *ApJ* 249, 254.

Sorkin, R. D., Jun. 1982. A Stability Criterion for Many Parameter Equilibrium Families. *ApJ* 257, 847.

Stergioulas, N., Jun. 2003. Rotating Stars in Relativity. *Living Reviews in Relativity* 6, 3.

Takami, K., Rezzolla, L., Yoshida, S., Sep. 2011. A quasi-radial stability criterion for rotating relativistic stars. *MNRAS* 416, L1–L5.

Tolman, R. C., Apr. 1930. On the Weight of Heat and Thermal Equilibrium in General Relativity. *Physical Review* 35, 904–924.

Tolman, R. C., Feb. 1939. Static Solutions of Einstein’s Field Equations for Spheres of Fluid. *Physical Review* 55, 364–373.

Torok, G., Bakala, P., Stuchlik, Z., Cech, P., Mar. 2008. Modeling the Twin Peak QPO Distribution in the Atoll Source 4U 1636-53. *Acta Astronomica* 58, 1–14.

Trümper, J. E., Jul. 2011. Observations of neutron stars and the equation of state of matter at high densities. *Progress in Particle and Nuclear Physics* 66, 674–680.

Trümper, J. E., Burwitz, V., Haberl, F., Zavlin, V. E., Jun. 2004. The puzzles of RX J1856.5-3754: neutron star or quark star? *Nuclear Physics B Proceedings Supplements* 132, 560–565.

Weber, F., Glendenning, N. K., May 1992. Application of the improved Hartle method for the construction of general relativistic rotating neutron star models. *ApJ* 390, 541–549.

Appendix A. The Hartle solution and equatorial circular orbits

Appendix A.1. The Hartle-Thorne vacuum solution

It is possible to write the Hartle-Thorne metric given by eq. 6 in an analytic closed-form in the exterior vacuum case as function of the total mass M , angular momentum J , and quadrupole moment Q of the rotating star. The angular velocity of local inertial frames $\omega(r)$, proportional to Ω , and the functions h_0, h_2, m_0, m_2, k_2 , proportional to Ω^2 , are derived from the Einstein equations (see Hartle, 1967; Hartle and Thorne, 1968, for details). Following this

prescriptions the eq. 6 become:

$$\begin{aligned}
ds^2 = & \left(1 - \frac{2M}{r}\right) \left[1 + 2k_1 P_2(\cos \theta)\right. \\
& + 2 \left(1 - \frac{2M}{r}\right)^{-1} \frac{J^2}{r^4} (2 \cos^2 \theta - 1) \left. \right] dt^2 \\
& + \frac{4J}{r} \sin^2 \theta dt d\phi - \left(1 - \frac{2M}{r}\right)^{-1} \\
& \times \left[1 - 2 \left(k_1 - \frac{6J^2}{r^4}\right) P_2(\cos \theta)\right. \\
& - 2 \left(1 - \frac{2M}{r}\right)^{-1} \frac{J^2}{r^4} \left. \right] dr^2 \\
& - r^2 [1 - 2k_2 P_2(\cos \theta)] (d\theta^2 + \sin^2 \theta d\phi^2), \quad (\text{A.1})
\end{aligned}$$

where

$$\begin{aligned}
k_1 = & \frac{J^2}{Mr^3} \left(1 + \frac{M}{r}\right) + \frac{5}{8} \frac{Q - J^2/M}{M^3} Q_2^2(x), \\
k_2 = & k_1 + \frac{J^2}{r^4} + \frac{5}{4} \frac{Q - J^2/M}{M^2 r \sqrt{1 - 2M/r}} Q_2^1(x),
\end{aligned}$$

and

$$\begin{aligned}
Q_2^1(x) = & (x^2 - 1)^{1/2} \left[\frac{3x}{2} \ln \left(\frac{x+1}{x-1} \right) - \frac{3x^2 - 2}{x^2 - 1} \right], \\
Q_2^2(x) = & (x^2 - 1) \left[\frac{3}{2} \ln \left(\frac{x+1}{x-1} \right) - \frac{3x^3 - 5x}{(x^2 - 1)^2} \right],
\end{aligned}$$

are the associated Legendre functions of the second kind, being $P_2(\cos \theta) = (1/2)(3 \cos^2 \theta - 1)$ the Legendre polynomial, and where it has been effectuated the re-scaling $x = r/M - 1$. The constants M , J and Q are the total mass, angular momentum and mass quadrupole moment of the rotating object, respectively. This form of the metric corrects some misprints of the original paper by Hartle and Thorne (1968) (see also Berti et al., 2005; Boshkayev et al., 2012a). To obtain the exact numerical values of M , J and Q , the exterior and interior metrics have to be matched at the surface of the star. It is worthy underline that in the terms involving J^2 and Q , the total mass M can be substituted by $M^{J=0}$ since δM is already a second order term in the angular velocity.

Appendix A.2. Angular velocity of equatorial circular orbits

It is possible to obtain the analytical expression for the angular velocity Ω given by Eq. (20) with respect to an observer at infinity, taking into account the parameterization of the four-velocity u of a test particle on a circular orbit in equatorial plane of axisymmetric stationary spacetime, regarding as parameter the angular velocity Ω itself:

$$u = \Gamma [\partial_t + \Omega \partial_\phi], \quad (\text{A.2})$$

where Γ is a normalization factor such that $u^\alpha u_\alpha = 1$. Normalizing and applying the geodesics conditions we get

the following expressions for Γ and $\Omega = u^\phi/u^t$

$$\Gamma = \pm (g_{tt} + 2\Omega g_{t\phi} + \Omega^2 g_{\phi\phi})^{-1/2}, \quad (\text{A.3})$$

$$g_{tt,r} + 2\Omega g_{t\phi,r} + \Omega^2 g_{\phi\phi,r} = 0. \quad (\text{A.4})$$

Thus, the solution of Eqs. (A.3–A.4) can be written as

$$\Omega_{\text{orb}}^\pm(r) = \frac{u^\phi}{u^t} = \frac{-g_{t\phi,r} \pm \sqrt{(g_{t\phi,r})^2 - g_{tt,r} g_{\phi\phi,r}}}{g_{\phi\phi,r}}, \quad (\text{A.5})$$

where $+/-$ stands for co-rotating/counter-rotating orbits, u^ϕ and u^t are the angular and time components of the four-velocity respectively, and a colon stands for partial derivative with respect to the corresponding coordinate. To determine the mass shedding angular velocity (the Keplerian angular velocity) of the neutron stars, we need to consider only the co-rotating orbit, so from here and thereafter we take into account only the plus sign in Eq. (A.3) and we write $\Omega_{\text{orb}}^+(r) = \Omega_{\text{orb}}(r)$.

For the Hartle external solution given by Eq. (A.1) we obtain Eq. (20) with

$$\begin{aligned}
F_1 = & \left(\frac{M}{r}\right)^{3/2}, \\
F_2 = & \frac{48M^7 - 80M^6 r + 4M^5 r^2 - 18M^4 r^3}{16M^2 r^4 (r - 2M)} \\
& + \frac{40M^3 r^4 + 10M^2 r^5 + 15M r^6 - 15r^7}{16M^2 r^4 (r - 2M)} + F, \\
F_3 = & \frac{6M^4 - 8M^3 r - 2M^2 r^2 - 3M r^3 + 3r^4}{16M^2 r (r - 2M)/5} - F, \\
F = & \frac{15(r^3 - 2M^3)}{32M^3} \ln \frac{r}{r - 2M}.
\end{aligned}$$

The maximum angular velocity possible for a rotating star at the mass-shedding limit is the Keplerian angular velocity evaluated at the equator ($r = R_{\text{eq}}$), i.e.

$$\Omega_K^{J \neq 0} = \Omega_{\text{orb}}(r = R_{\text{eq}}). \quad (\text{A.6})$$

In the static case i.e. when $j = 0$ hence $q = 0$ and $\delta M = 0$ we have the well-known Schwarzschild solution and the orbital angular velocity for a test particle $\Omega_K^{J=0}$ on the surface ($r = R$) of the neutron star is given by

$$\Omega_K^{J=0} = \sqrt{\frac{M^{J=0}}{R_{M^{J=0}}^3}}. \quad (\text{A.7})$$